This is a repository copy of *Multilevel DC-Link Converter Photovoltaic System with Modified PSO Based on Maximum Power Point Tracking*.

White Rose Research Online URL for this paper:
http://eprints.whiterose.ac.uk/116025/

Version: Accepted Version

Multilevel DC-Link Converter Photovoltaic System with Modified PSO Based on Maximum Power Point Tracking

Mingxuan Mao[1,2], Li Zhang[2], Qichang Duan[1], Benjamin Chong[2]

[1]Automation College, Chongqing University, Chongqing 400044, China

[2]School of Electronic and Electrical Engineering, University of Leeds

Leeds LS2 9JT, United Kingdom

Abstract: The paper presents a modified particle swarm optimization (MPSO) control strategy for the maximum power point tracking applied to a multilevel DC-link PV power generation system. This system consists of a chain of PV modules with individual DC-DC converters and has a DC-AC converter at its terminals for generating AC voltage. The proposed MPSO control method can predict all PV voltages at their maximum power point on the basis of respective light level and temperature. A PWM with permutation of DC converter switching is applied to balance switch utilization. The method is applied to a system of five-voltage levels with two PV-converter units under different light intensities and the results are compared with the perturb and observe (P&O) method and the traditional PSO method under the same operating conditions. The paper shows that the new method gives more rapid convergence, increased power output, and lower total harmonic distortion.

1   Introduction

PV power generators are now widely installed in residential areas and commercial centers for supplying electricity to local users as well as to the utility grid. They are usually constructed

by connecting many PV cells of the same type in series chains. These long chains of PV cells incur operational complications; the characteristics of the chained PV cells are not identical, hence they may not conduct the same current at their operating points. The cells which are least efficient set the safe operating current of the string. A more serious problem occurs when illumination of the chains is uneven, i.e. a subset of the PV cells is shaded. The current must be limited to the maximum forward current in the shaded set to avoid driving any of these into a reverse voltage condition. This always absorbs power and can result in reverse breakdown and overheating. The use of by-pass diodes has limited this problem, but power potentially available from by-passed cells is lost. Various control methods, such as such as perturb and observe (P&O) (Femia et al.,2009; Killi and Samanta, 2015; Elbaset et al., 2016), Incremental conductance (IncCond) (Elgendy et al., 2012; Radjai et al., 2014; Li et al., 2016), hill climbing (HC) (Alajmi et al., 2011; Xiao et al., 2016), fuzzy logic (Messai et al., 2011; Letting et al., 2012; Cheng et al., 2015; Rezvani and Gandomkar, 2016), artificial neural network (ANN) (Liu et al., 2013; Boumaaraf et al. 2015; Lin et al., 2016; Messalti et al., 2017), particle swarm optimization (PSO) (Ishaque et al., 2012; Cheng et al., 2015; Letting et al., 2012; Manickam et al., 2016; Renaudineau et al., 2015), sliding mode (Kim, 2007; Chu and Chen, 2009; Zhang et al., 2015; Mojallizadeh et al., 2016; Ouchen et al., 2016) and so on, have been proposed to enable optimal power generation from the chained PV strings with by-pass diodes and under partial shading conditions, but satisfactory solutions in terms of simultaneously maximizing the power generated and protecting the PV panels have still been a challenge (Rezk and Eltamaly, 2015; Chen et al., 2015; Liu et al., 2016; Kumar and Chatterjee, 2016; Gupta et al., 2016).

The approach of connecting a PV module with a DC-DC converter, cascading many such units in a chain, and generating a multilevel DC output voltage may provide a solution. The benefit of this configuration is clear, since the individual PV modules can be controlled for maximum power output according to their respective light levels and characteristics. The same total chain current flows through the converter switches, but is no longer the same as the individual PV currents, and high power dissipation problems caused by shaded PV cells can be

prevented. With continuously falling cost of power semiconductor devices, this type of configuration should become commercially viable. Various configurations for generating multilevel DC-voltage by chained PV-Converter units have been proposed in the literature including the work initiated by Shimizu et al. (Shimizu et al., 2001; Abdalla et al., 2016; Busquets-Monge et al., 2008; Gao et al., 2009; Velasco-Quesada et al., 2009; Renaudineau et al., 2015). Zhang et al. (Zhang et al., 2009) proposed the scheme which uses fly-back converters for each PV source. The drawback of this is that the individual PV sources cannot be controlled completely independently, hence locating the MPP of one PV source does not mean that the other PV source can be operating at its MPP. In (Renaudineau et al., 2015), architecture, including one dc/dc converter for each PV generator, is considered. The converters' output terminals are series connected to a high-voltage dc bus, where also a bidirectional dc/dc converter managing the power from/to a storage device is plugged, and then the real-time constrained optimization problem is solved by using the particle swarm optimization method, which needs the knowledge of the actual current versus voltage curve of each PV generator. A system proposed by Abdalla *et al* (Abdalla et al., 2016) uses step-down DC-DC converters for each PV module, and can achieve independent control for each PV module. However the control of this type of configuration can be challenging since it needs to track the MPPs of all the PV modules and control their corresponding converters simultaneously. In addition, the well-known perturb and observe (P&O) method is applies to the scheme to control each PV-converter unit, but this makes the system slow to converge to the MPPs and the output voltages of all the PV modules oscillate during the searching process.

This paper presents a new MPPT control strategy based on a modified particle swarm optimization (MPSO) for the multilevel DC-link PV system proposed in (Abdalla et al., 2016)

operating under PSCs and load variations. PSO is an evolutionary computation algorithm and has been applied for MPPT of PV systems in some investigations (Ishaque et al., 2012; Koad et al., 2016; Manickam et al., 2016; Seyedmahmoudian et al., 2015; Sundareswaran et al., 2015; Liu et al., 2012; Babu et al., 2015), but none of these treat the multilevel DC-link PV converter system. In this context the benefit of using the MPSO is clear; it can predict all the PV-Converter voltages at their respective MPPs as defined by their light levels quickly and without disturbing the system. The predicted voltages are applied to control the individual DC-DC converters simultaneously. In this paper a permutation PWM scheme is applied to control the multiple module terminal converters, so that switching utilisation can be balanced. In addition the output of the whole converter chain is connected to a DC-AC voltage source converter, providing a suitable AC output for grid connection.

The rest of the paper is organized as follows: Section 2 presents in detail the new optimal control scheme based on permutation of PV sources combined with the modified PSO – based MPPT method. The structure of the PV system based on multilevel DC-Link converters is described in Section 3. Section 4 presents and discusses the experimental results, with conclusions in Section 5.

2 Structure of the PV System based on Multilevel DC-Link Converter

Figure 1 shows the configuration of a PV system comprising two PV units acting in conjunction with a multilevel DC-link converter. Each PV unit consists of a single PV source, a capacitor and a switch with a complimentary diode (Abdalla et al., 2016). In Figure 1, In_x represents the different inputs. The units are connected in series and any of them can be switched in or out of the chain by turning on or off its switch. When a unit is switched off, it is being bypassed by a diode. The two switches (SW1, SW2) operate at a high frequency and are controlled by the direct PWM method (Dai et al., 2005) to form a three-level positive DC voltage. The H–bridge inverter at the output serves to convert the multilevel DC voltage

waveform to alternative positive and negative output voltage half-cycles of the required output frequency (e.g. 50Hz). The generation of multiple voltage levels, combined with proper control, enables forming the approximate sinewave output (Abdalla et al., 2016).
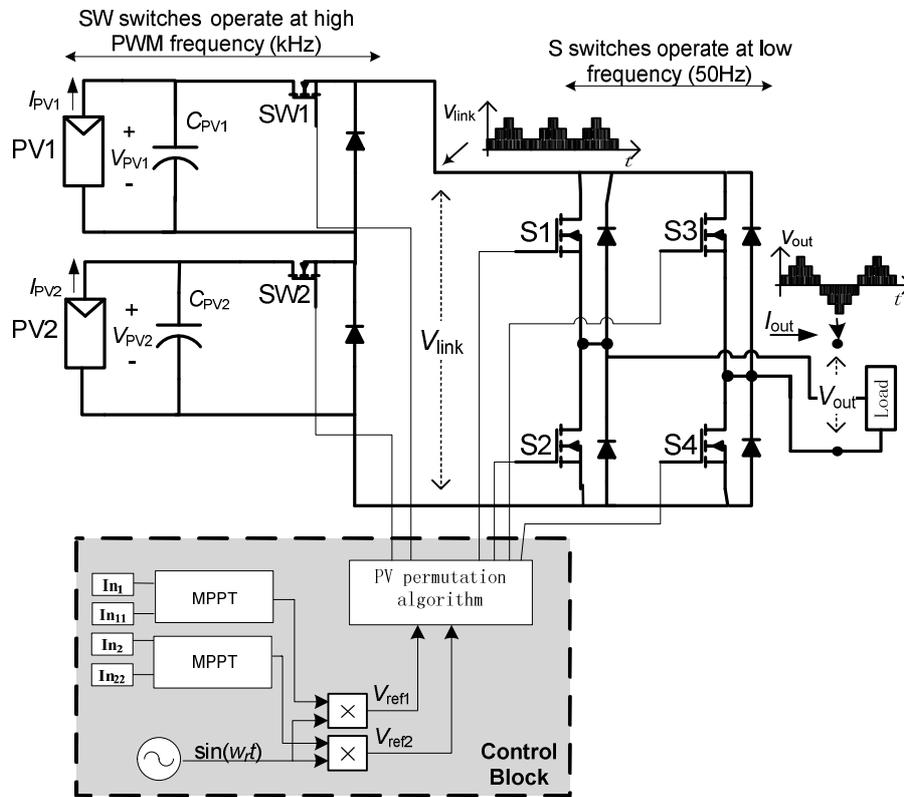

Figure 1 PV system with multilevel DC- link converter and the MPPT method

3 Optimal Control Scheme based on Permutation of PV Sources

The optimal control scheme should maximise the power transferred from PV sources to the AC load or grid in different light conditions, and generate a nearly sinusoidal voltage with minimum harmonic distortion and DC offset. Ideally, it should also ensure equal switching utilisation and hence the losses. The solution presented in this paper comprises two parts: (i) the modified PSO based-MPPT algorithm for generation of the MPP reference voltage and (ii) PWM algorithm with permutation of PV sources for switching control.

3.1 Modified PSO Based-MPPT algorithm

Under PSCs and load variation, the terminal voltage of PV system with a simple search method may oscillate around a MPP, and the system may lose the MPP during rapid irradiance changes. To address this issue, the detailed methods for MPPT control will be introduced in this section. The proposed algorithm combines the extended memory searching capabilities and the adaptive inertia weight of MPSO, which is performed by a boost DC/DC converter to quickly and accurately search for the MPPs and reduce the voltage ripple and increase the power output under different partial shading conditions. In addition, the proposed algorithm can rapidly search the MPP, and set the MPP as the initial position to track the accuracy MPP dynamically. The proposed algorithm is helpful to enhance efficiency and minimize errors for the MPPT problem under PSCs and load variation. The procedure and the equations of the proposed MPSO algorithm are detailed as follow.

3.1.1 Principles of PSO Algorithm

PSO is an evolutionary computation technique proposed by Kennedy and Eberhart in 1995 (Eberhart and Kennedy, 1995). Originated from observing the behavior of the bird flocks, which and is used to solve the optimization issues, and in PSO particles, each particle represents a potential solution, which is corresponding to a fitness values based on fitness function. The standard PSO is shown as follows:

$$v_{t+1} = \omega \, v_t + \alpha_t^l \left(p_t^l - x_t \right) + \alpha_t^g \left(p_t^g - x_t \right) \tag{1}$$

$$x_{t+1} = x_t + v_{t+1} \tag{2}$$

where subscript t denotes the index of iteration; v_t represents the speed of the particle in the tth iterative process; x_t represents the position of the particle in the tth iterative process; p_t^l represents the current local extreme value point of the particle in the tth iterative process; p_t^g

represents the current global extreme value point of the population in the tth iterative process; ω is known as the inertia weight; c_1 and c_2 are treated as the acceleration factors, and $\alpha_t^l = c_1 r_1$, $\alpha_t^g = c_2 r_2$, r_1, $r_2 \sim U(0,1)$, ω, α_t^l, $\alpha_t^g \in R$, $\alpha_t^l \sim U(0,c_1)$, $\alpha_t^g \sim U(0,c_2)$.

3.1.2. PSO with Extended Memory (PSOEM)

Although the traditional PSO algorithm can have good performance in most cases, there are still some defects needed to solve, such as prior low precision, slow late convergence and relapsing into local optimization. PSOEM combines several improved PSO algorithms, making full use of their advantages (Duan et al., 2016). From a psychological point of view, expanded memory means that the individual accumulates the search experience, which is conducive to improve the convergence speed. PSOEM can be expressed as follows (Duan et al., 2016):

$$v_{t+1} = \omega \, v_t + \alpha_t^l \left[\xi_t \left(p_t^l - x_t \right) + \xi_{t-1} \left(p_{t-1}^l - x_{t-1} \right) \right]$$
$$+ \alpha_t^g \left[\xi_t \left(p_t^g - x_t \right) + \xi_{t-1} \left(p_{t-1}^g - x_{t-1} \right) \right] \tag{3}$$

where p_{t-1}^l represents current extreme value point of the particle in the $t\text{-}1^{th}$ iterative process; p_{t-1}^g represents the current global extreme value point of the population in the $t\text{-}1^{th}$ iterative process; ξ_t is called current effective factor; ξ_{t-1} is called effective factor of extended memory, and $x_{t+1} = x_t + v_{t+1}$, $\xi_t, \xi_{t-1} \in R^+$, $\sum \xi_i = 1$. In particular, when $\xi_{t-1} = 0$, that is, $\xi_t = 1$, then (3) = (1). In this sense, PSO is a special case of PSOEM.

3.1.3 The proposed algorithm with adaptive inertia weight

Given its simple concept and effectiveness, the PSO has become a popular optimizer and has widely been applied in practical problem solving (Zhan et al., 2009). Meanwhile, much research on performance improvements has been reported, including parameter studies, combination with auxiliary operations, and topological structures (Eberhart and Shi, 2004).

According to Shi and Eberhart's analysis in (Shi and Eberhart, 1998), the inertia weight is critical in balancing global and local search. A larger inertia weight facilitates global exploration while a smaller one facilitates local exploitation (Shi and Eberhart, 1998). It controls the balance between exploration (global search state) and exploitation (local search state) (Wu et al., 2015). Furthermore, implementing a damping mechanism to ω contributes to better global exploration in the initial stages, and better local exploitation when the swarm is closer to the source (Zou et al., 2015). Therefore, aimed to the nonlinear and multiple peaks characteristics of the output P-V curves in PV system under PSCs, the linearly decreasing ω with the iterative generation proposed in (Shi and Eberhart, 1999) is used to overcome the multiple local MPPs and further improve the effectiveness of GMPPT under different PSCs. The inertia weight is described by the following equation:

$$\omega = \omega_{max} - \left(\omega_{max} - \omega_{min}\right)\frac{g}{G} \tag{4}$$

where g is the generation index representing the current number of evolutionary generations, and G is a predefined maximum number of generations. Here, the maximal and minimal weights ω_{max} and ω_{min} are set according to the need.

3.1.4 Stability analysis of PSO and the proposed algorithm

One of hot issue in present research about PSO algorithm is the stability analysis. From the perspective of discrete control theory, the stability region of PSO and the proposed algorithm is presented as follow:

First of all, we assume that

$$\bar{x}_t = p_t^g - x_t \tag{5}$$

By using that, we have

$$p_t^l - x_t = \left(p_t^l - p_t^g \right) + \overline{x}_t \tag{6}$$

Eqs. (1) and (5) can be combined and written as follow:

$$v_{t+1} = \omega v_t + \alpha_t^l \left[\left(p_t^l - p_t^g \right) + \overline{x}_t \right] + \alpha_t^g \overline{x}_t = \omega v_t + \alpha_t \overline{x}_t + \alpha_t^l \left(p_t^l - p_t^g \right) \tag{7}$$

where, $\alpha_t = \alpha_t^l + \alpha_t^g$.

According to Eq.(5), $\overline{x}_{t+1}$ can be explained as follow:

$$\overline{x}_{t+1} = p_{t+1}^g - x_{t+1} \tag{8}$$

Furthermore, Eqs. (2) and (7) can be combined as follow:

$$\overline{x}_{t+1} = \left(1 - \alpha_t \right) \overline{x}_t - \omega v_t - \alpha_t^l \left(p_t^l - p_t^g \right) + p_{t+1}^g - p_t^g \tag{9}$$

By merging Eqs.(8) and (9), the vector matrix form of PSO algorithm is

$$\begin{bmatrix} \overline{x}_{t+1} \\ v_{t+1} \end{bmatrix} = A_0 \begin{bmatrix} \overline{x}_t \\ v_t \end{bmatrix} + b_0 \tag{10}$$

where, $A_0 = \begin{bmatrix} \left(1 - \alpha_t \right) & -\omega \\ \alpha_t & \omega \end{bmatrix}$, $b_0 = \begin{bmatrix} M_0 & N_0 \end{bmatrix}^T$, $M_0 = -\alpha_t^l \left(p_t^l - p_t^g \right) + p_{t+1}^g - p_t^g$, and

$N_0 = \alpha_t^l \left(p_t^l - p_t^g \right)$. In addition, Eq.(10) represents the state space equation of PSO algorithm,

A_0 is coefficient matrix.

For ease of analysis, we define: $\xi_t = \xi_{t-1} = \dfrac{1}{2} \displaystyle\sum_{i=0}^{1} \xi_{t-i}$.

Furthermore, we assume:

$$\overline{x}_t = \frac{1}{2} \left(p_t^g - x_t \right) + \frac{1}{2} \left(p_{t-1}^g - x_{t-1} \right) \tag{11}$$

Similarly, the vector matrix form of the proposed algorithm is shown as follow

$$\begin{bmatrix} \overline{x}_{t+1} \\ \overline{x}_t \\ v_{t+1} \\ v_t \end{bmatrix} = A_1 \begin{bmatrix} \overline{x}_t \\ \overline{x}_{t-1} \\ v_t \\ v_{t-1} \end{bmatrix} + b_1 \tag{12}$$

$$A_1 = \begin{bmatrix} \left(1 - \dfrac{1}{2}\alpha_t\right) & -\dfrac{1}{2}\alpha_{t-1} & -\dfrac{1}{2}\omega & -\dfrac{1}{2}\omega \\ 1 & 0 & 0 & 0 \\ \alpha_t & 0 & \omega & 0 \\ 0 & 0 & 1 & 0 \end{bmatrix} \quad b_1 = \begin{bmatrix} M_1 & 0 & N_1 & 0 \end{bmatrix}^T$$

where,

$$N_1 = \frac{1}{2}\alpha_t^l \sum_{i=0}^{1}\left(p_{t-i}^l - p_{t-i}^g\right) \quad , \quad M_1 = -\frac{1}{4}\sum_{i=0}^{1}\alpha_{t-i}^l \sum_{j=i}^{i+1}\left(p_{t-j}^l - p_{t-j}^g\right) + \frac{1}{2}\left(p_{t+1}^g - p_{t-1}^g\right).$$

In order to simplify the stability analysis of PSO and the proposed algorithm, we assume that α_t and α_{t-1} are real constant, and $\alpha_t = \alpha_{t-1}$. The stability region of PSO and the proposed algorithm can be obtained by using their coefficient matrix (A_0 and A_1) respectively.

The characteristic equation of A_0 is

$$\lambda^2 + \left(\alpha_t - \omega - 1\right)\lambda + \omega = 0 \tag{13}$$

When the characteristic root is in the unit circle, its stability region is [45]:

$$S_0 = \left\{(\omega, \alpha_t) : |\omega| < 1, 0 < \alpha_t < 2(\omega + 1)\right\} \tag{14}$$

Meanwhile, the characteristic equation of A_1 is

$$\lambda^4 + \left(\frac{1}{2}\alpha_t - \omega - 1\right)\lambda^3 + \left(\frac{1}{2}\alpha_t + \omega\right)\lambda^2 = 0 \tag{15}$$

Eq. (15) can be simplified as follow:

$$\lambda^2 + \left(\frac{1}{2}\alpha_t - \omega - 1\right)\lambda + \frac{1}{2}\alpha_t + \omega = 0 \tag{16}$$

When the characteristic root is in the unit circle, its stability region is

$$S_1 = \left\{(\omega, \alpha_t) : |\omega| < 1, 0 < \alpha_t < 2(1 - \omega)\right\} \tag{17}$$

The stability region of PSO and the proposed algorithm is shown in Figure 2, in which the light gray area represents the real number root, and the dark gray area represents the complex root. The dividing line between the real root and the complex root is a parabola of which the discriminant equals zero. Obviously, it can be clearly seen from Figure 2 that the stability region of the two algorithms is equal.
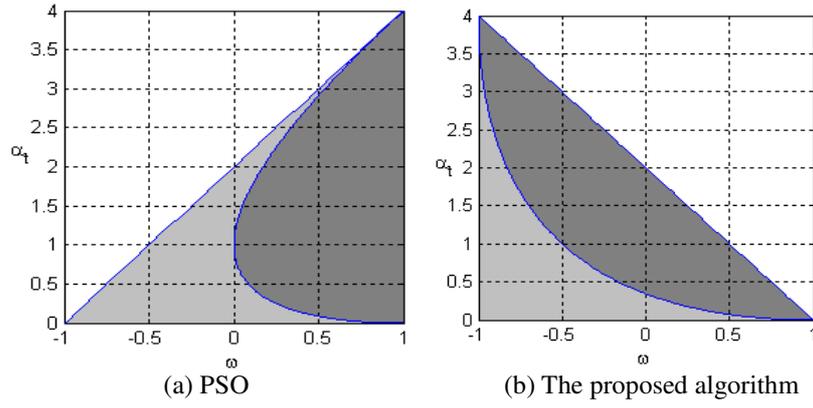
(a) PSO   (b) The proposed algorithm

Figure 2 Stability Region of PSO and the proposed algorithm

3.1.5 Fitness function for the proposed MPPT algorithm

Taking the branch current as the optimization variables, the fitness function is P-I relationship of the series branch, as shown in formula (18) and formula (19).

$$fit = I \times \sum_{k=1}^{n_s} PVprog(i_k, Sun_k, T_k), n_z = 10 \tag{18}$$

$$PVprog(I, Sun, T) = 1.1103 \times log_{10}(\frac{3.8 \times Sun - I + 2.2 \times 10^{-8}}{2.2 \times 10^{-8}}) - 0.2844 \times I \tag{19}$$

where *PVprog(I, Sun, T)* represents the output power of each of PV panels-current characteristic function, *Sun* and *T* respectively represent light intensity and environment temperature.

3.1.6 The proposed MPPT algorithm

From the above, the flowchart of the proposed algorithm is shown in Figure 3. From the above, the proposed MPPT method is applied in sequence to each PV unit at each sampling instant, to track individually their respective reference voltages. This may lead to different voltage values depending on the weather conditions and PV panel characteristics.

The specific process of the proposed MPPT method is shown as follows:

i) Initialize the position and speed of the fish, the optimal locations of each fish's memory and the optimal position parameters recorded on bulletin board;

ii) Test the 4 kinds of combination behavior patterns: cluster or foraging, collision or foraging, memory or foraging and communication or foraging;

iii) Select the optimal combination behavior model from ii) and use the velocity update current location of the artificial fish;

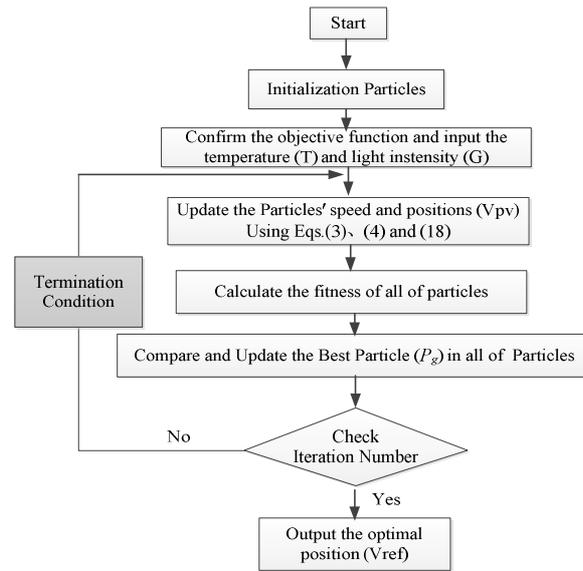iv) If the specified number of iterations is available, the optimization will end, otherwise going to step ii).

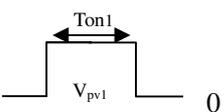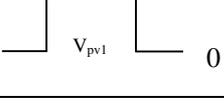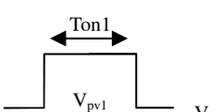Figure 3 Flowchart of the proposed MPPT method

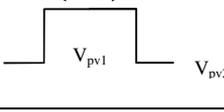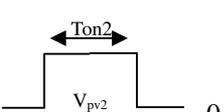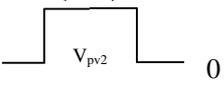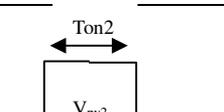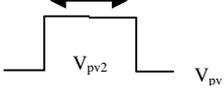**3.2 PWM Algorithm with Permutation of PV Sources**

For maximum power extraction, the terminal voltage of each PV unit should be as close as possible to its individual reference voltage established by the TSPSO based-MPPT method process. A PWM algorithm based on permutation of PV sources has been used to meet the criteria of equal switch utilisation and low waveform distortion, which consists of three stages (Abdalla et al., 2016; Dai et al., 2005): i) the direct PWM determines the output voltage levels and switch-on time intervals in the first stage; ii) the sequential permutation algorithm is implemented to determine the switching states of all PV units for building up the output voltage of the system in the second stage; iii) the H-bridge converter is used to change the multilevel DC voltage waveform to a single-phase AC waveform of low frequency by tracking the

sinusoidal reference signal in the last stage.

For clarification, a graphical illustration of the process for generating the output waveform in the basic system with two PV sources is given in Table 1. Table 1 presents the switching states and output voltage generation for the system with two PV sources ($n = 2$), and gives a more practical demonstration of the generated output voltage through the permutation algorithm, and in each case the non-controlled PV source is used to form the basis voltage for the controlled PV source. Furthermore, Figure 4 contains the whole process of the algorithm for two PV sources (reference signals, switch control signals, output voltage) (Abdalla et al., 2016). In Figure 4, v_{ref1} and v_{ref2} are two reference voltages of the five-level converter. These signals are sampled at periods T_{s} yielding M_{f} samples for each reference signal over the time period $T_{\mathrm{r}} = 1/f_{\mathrm{r}}$.

Table 1 Output Generation from Two PV Sources

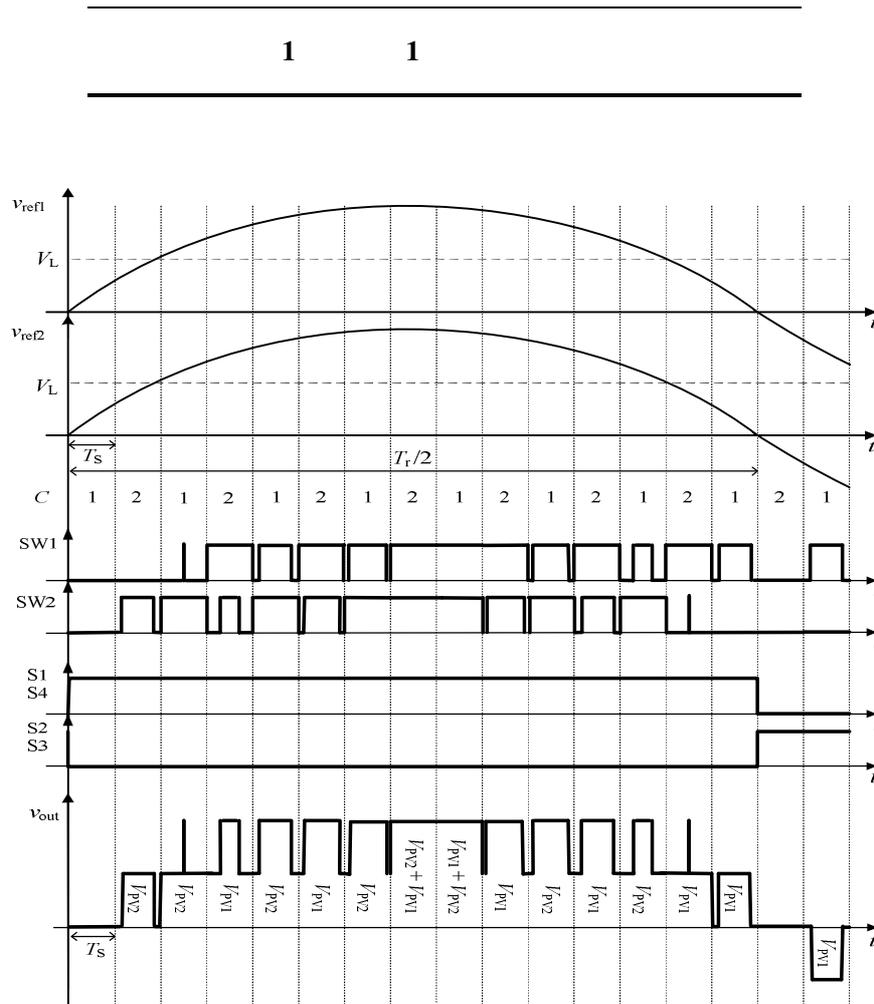| C	$v_{\mathbf{offset1}}$	$v_{\mathbf{offset2}}$	Output generation per switching period T_s
1	0	0	SS — waveform: V_{pv1} pulse with $Ton1$, baseline 0 to 0
	1	0	0 — waveform: V_{pv1} pulse with $Ton1$, baseline 0 to 0
	0	1	waveform: V_{pv1} pulse with $Ton1$, baseline V_{pv2} to V_{pv2}
	1	1	V_{pv2} — waveform: V_{pv1} pulse with $Ton1$, V_{pv2}
2	0	0	waveform: V_{pv2} pulse with $Ton2$, baseline 0 to 0
	0	1	0 — waveform: V_{pv2} pulse with $Ton2$, baseline 0 to 0
	1	0	V_{pv1} — waveform: V_{pv2} pulse with $Ton2$, baseline V_{pv1} to V_{pv1}

Figure 4 Graphical illustration of the process for generating the output waveform in the basic

system with two PV sources

4 Simulation Results

4.1 Numerical simulation analysis of the proposed MPPT algorithm

To evaluate and analyze the performance of the proposed algorithm, we perform numerical

simulation with Matlab7.1. A number of numerical simulation experiments are done on 3

benchmark functions to compare its performance with the PSO algorithm under the same

parameter settings. Parameter settings of the proposed algorithm are shown in Table 2, and

benchmark functions with their optimum value (column 3) and search range (column 5) are

presented in Table 3. In addition, we use 3 benchmark functions with D=10, 30, 50, as listed in

Table 3. These scalable benchmark functions in Table 3 involve different types of problems such as the continuous unimodal function Sphere, and the multimodal functions Rastrigin and Griewank. Furthermore, two algorithms run 100 times independently, the population size is 100 and the maximum number of iteration is 1000, 2000 and 300 respectively in the cases of the low-, middle- and high-dimensional benchmark functions. And the reported results are the M_iteration, Success ratio and E_number of the statistical experimental data.

Table 4 shows the M_iteration, Success ratio and E_number of obtained by each algorithm for 3 benchmark functions. M_iteration represents the number of iteration when algorithm converges to the optimal value. Success ratio is the optimizing success rate. E_number represents the number of iteration that benchmark function is expected to, which is one of the main evaluations of algorithm performance in practical applications. From Table 4, it is clear that the proposed algorithm consistently outperforms the PSO algorithm in most cases. This can be explained that the proposed algorithm could make use of the searching extended capabilities of the extended memory and the self-learning ability to optimize the searching process and improve the convergence precision.

Table 2 Parameter Settings of the proposed algorithm

Algorithm	$\left(\xi_t, \xi_{t-1}\right)$
PSOEM$_1$	(0.1,0.9)
PSOEM$_2$	(0.2,0.8)
PSOEM$_3$	(0.3,0.7)
PSOEM$_4$	(0.4,0.6)
PSOEM$_5$	(0.5,0.5)
PSOEM$_6$	(0.6,0.4)
PSOEM$_7$	(0.7,0.3)
PSOEM$_8$	(0.8,0.2)
PSOEM$_9$	(0.9,0.1)

Table 3 Parameter Settings of Benchmark Functions

Name	Function	Optimal value	Threshold value	Search range
Sphere	$f(x)=\sum_{i=1}^{n} x_i^2$	0	0.01	[-100,100]
Rastrigin	$f(x)=\sum_{i=1}^{n}\left(x_i^2 - 10\cos(2\pi x_i)+10\right)$	0	100	[-5.12,5.12]
Griewank	$f(x)=\frac{1}{4000}\sum_{i=1}^{n} x_i^2 - \prod_{i=1}^{n}\cos\left(\frac{x_i}{\sqrt{i}}\right)+1$	0	0.15	[-600,600]

Table 4 Optimization results tested on three benchmark functions

Algorithm	Pop. size	Dim	Gene.	Sphere (M_iteration, Success ratio, E_number)	Rastrigin (M_iteration, Success ratio, E_number)	Griewank (M_iteration, Success ratio, E_number)
PSO	100	10	1000	(18.41,100%,1841.00)	(11.41,97%,1176.53)	(41.78,83%,5034.11)
		30	2000	(23.56,87%,2708.42)	(32.22,90%,3580.25)	(30.54,83%,3679.80)
		50	3000	(34.92,89%,3923.75)	(21.83,80%,2728.13)	(21.23,87%,2440.22)
PSOEM$_1$	100	10	1000	(5.86,100%,586.00)	(5.92,99%,597.90)	(5.05,100%,505.00)
		30	2000	(5.91,100%,591.00)	(5.87,99%,592.80)	(5.12,100%,512.00)
		50	3000	(5.91,100%,591.00)	(5.99,97%,617.49)	(5.13,98%,523.74)
PSOEM$_2$	100	10	1000	(5.63,100%,563.00)	(5.60,100%,560.00)	(5.02,98%,512.29)
		30	2000	(5.75,100%,575.00)	(5.73,100%,573.00)	(5.18,100%,500.00)
		50	3000	(5.72,100%,572.00)	(5.66,100%,566.00)	(5.00,100%,566.00)
PSOEM$_3$	100	10	1000	(5.26,100%,526.00)	(5.24,100%,524.00)	(4.93,100%,493.00)
		30	2000	(5.37,100%,537.00)	(5.39,100%,539.00)	(4.82,100%,482.00)
		50	3000	(5.37,100%,537.00)	(5.42,100%,542.00)	(5.98,100%,498.00)
PSOEM$_4$	100	10	1000	(5.10,100%,510.00)	(5.06,100%,506.00)	(5.13,99%,515.67)
		30	2000	(5.07,99%,512.19)	(5.14 ,100%,514.00)	(5.29 ,100%,529.00)
		50	3000	(5.14,100%,514.00)	(5.19,99%,524.44)	(5.42,99%,546.25)
PSOEM$_5$	100	10	1000	(5.01,100%,501.00)	(5.02 ,100%,502.00)	(5.37 ,99%,541.33)
		30	2000	(5.08,100%,508.00)	(5.13,100%,513.00)	(5.44,99%,547.60)
		50	3000	(5.16,99%,521.38)	(5.14,100%,514.00)	(5.06,98%,510.09)
PSOEM$_6$	100	10	1000	(5.04,100%,504.00)	(5.11,100%,511.00)	(6.37,100%,637.00)
		30	2000	(5.34,99%,539.74)	(5.27,99%,532.60)	(6.15,100%,615.00)
		50	3000	(5.47,99%,553.00)	(5.49,95%,578.39)	(6.65,99%,672.07)
PSOEM$_7$	100	10	1000	(5.13,100%,513.00)	(5.01,100%,501.00)	6.61,100%,661.00)
		30	2000	(5.13,100%,513.00)	(5.64,99%,569.33)	(6.25,100%,625.00)
		50	3000	(5.36,98%,546.65)	(5.34 ,99%,539.74)	(6.49 ,100%,649.00)
PSOEM$_8$	100	10	1000	(5.23,100%,523.00)	(5.32,100%,532.00)	(10.14,99%,1027.19)
		30	2000	(6.23,100%,623.00)	(6.24,99%,630.55)	(11.36,98%,1158.04)
		50	3000	(7.55,99%,762.17)	(6.54,100%,654.00)	(25.00,97%,2606.71)
PSOEM$_9$	100	10	1000	(6.85,100%,685.00)	(6.29,100%,629.00)	(14.57,97%,1500.32)

		30	2000	(9.01,100%,901.00)	(10.22,96%,1064.45)	(10.47,99%,1060.60)
		50	3000	(13.42,97%,1383.78)	(38.41,96%,4000.65)	(33.20,98%,3405.75)

4. 2 Empirical evaluations on the novel PV system

4.2.1 Simulation analysis under fast transient variations of shading patterns

Laboratory simulation experiments were performed on a system having two serially connected PV modules (sources) with 5-level converter as shown Figure 1. The parameters of the experimental system are listed in Table 5.

Table 5 PV system parameters used in simulations

Symbol	Parameter	Value
P_{mpp}	Maximum power of PV source	48.29W
V_{mpp}	Maximum voltage of PV source	16V
I_{mpp}	Maximum current of PV source	3.018A
C_{pv}	PV source terminal capacitor	2200μF
L	Load inductance	5mH
f	AC output frequency	50Hz

To evaluate the effectiveness of the proposed scheme with the novel MPPT algorithm, empirical tests are done on the PV system with the P&O method, the conventional PSO method and the proposed method under fast transient variations of shading patterns. The P&O method is set as the fixed step size (step size=1), and Table 6 shows the basic parameters used in the traditional PSO method and the proposed method, including the inertia weight ω, acceleration factors c_1 and c_2, maximum iterative number $Gene.$, number of particles S, the effective factor of extended memory ξ_{t-1} and current effective factor ξ_t.

Table 6 Parameter setting of the PSO and proposed methods

| Method	c_1	c_2	w	Gene.	S	ξ_{t-1}	ξ_t
PSO	2	2	0.9	50	20	--	--
Proposed Algorithm	2	2	self-adaption ($\omega_{max}=0.9, \omega_{min}=0.4$)	50	20	0.7	0.3

To study the algorithms five different light conditions are set for this PV system: Case 1, $G_1=1000W/m^2$, $G_2=600W/m^2$; Case 2, $G_1=1000W/m^2$, $G_2=800W/m^2$; Case 3, $G_1=1000W/m^2$, $G_2=350W/m^2$; Case 4, $G_1=1000W/m^2$, $G_2=900W/m^2$; Case 5, $G_1=1000W/m^2$, $G_2=500W/m^2$. Starting from case 1 initially, the switch to case 2 occurs at t = 2 sec., the switch to case 3 occurs at t = 4 sec., the switch to case 4 occurs at t = 8 sec., and case 4 to case 5 at t = 10 sec. as shown in Figure 5(a).
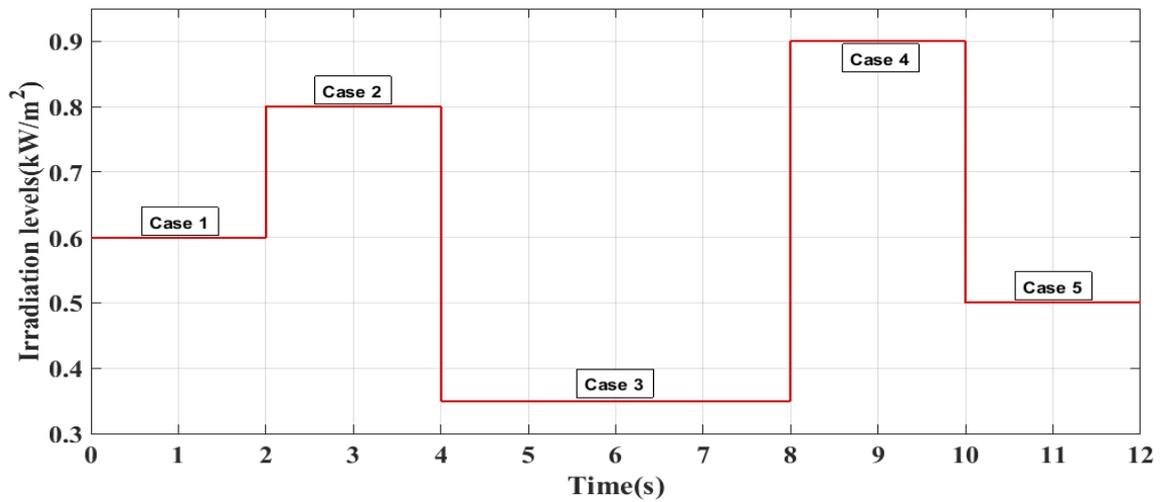
(a)
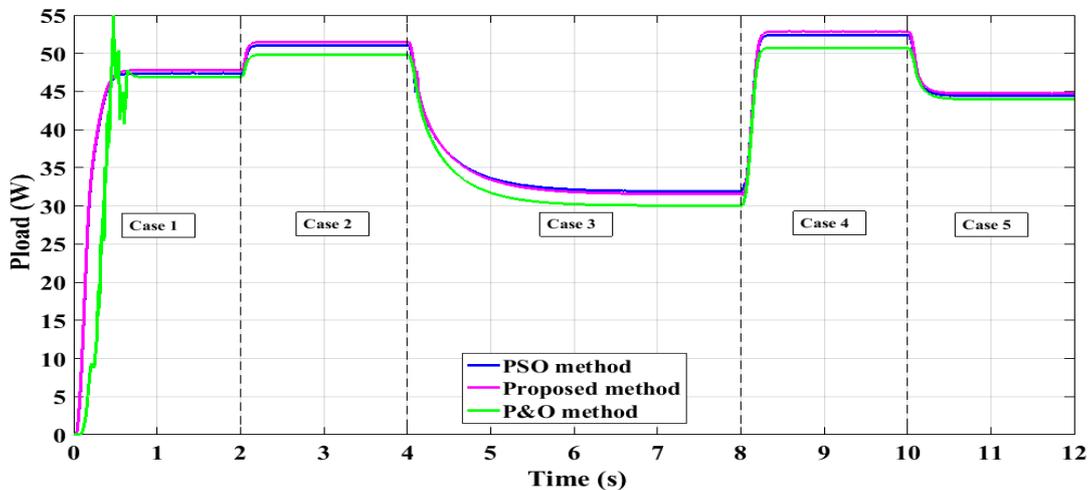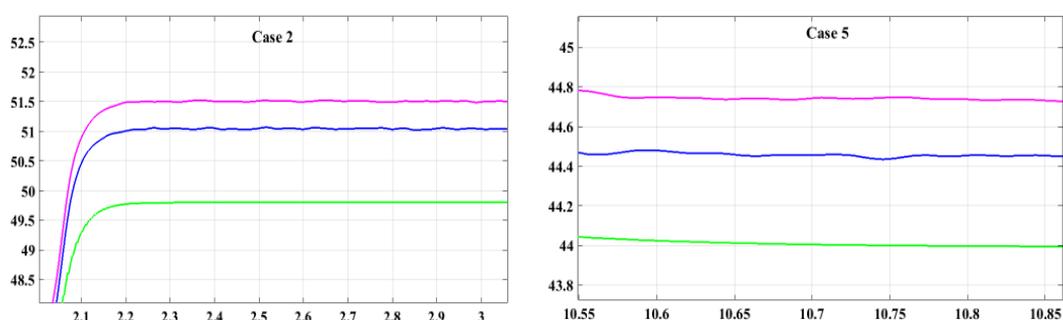
(b)
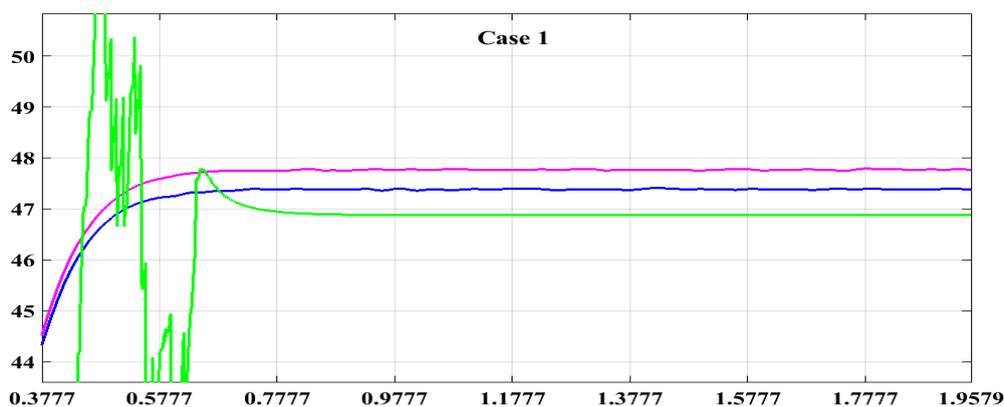
(c)

(d)   (e)

Figure 5 Experimental results of the three methods: (a) The changing process of illumination levels of the PV module; (b) Results from the three methods; (c) P_{load} curves of the three methods under Case 1; (d) P_{load} curves of the three methods under Case 2; (e) P_{load} curves of the three methods under Case 5.

Figure 5(b) shows the variations of output load power (P_{load}) of the PV system, using the P&O method, the traditional PSO algorithm, and the proposed method, under five fast transient variations of shading patterns. To vividly describe the advantage of the proposed method, Figures 5(c)-(e) show the output load power curves of the PV system under Case 1, Case 2 and Case 5 respectively. It can be clearly observed from Figure 5(c), compared to the traditional P&O algorithm, other two methods have less oscillation during the MPP searching processes. In

particular the output power converges to the peak points with little ripple. Also the proposed method converges much faster, taking only about 0.7sec. on average, but P&O's average time is about 0.85 sec. In addition, Figures 5(c)-(e) show that the proposed method obviously has more output load power than the other method, especially, in Case 2 and Case 5. From Figures 5(b)-(e), it is very obvious that the proposed algorithm is superior in the convergence speed, output accuracy and stability under different PSCs. This method can locate the precise MPP, reduce the oscillation and increase the output load power effectively.

4.2.2 Simulation analysis under different irradiance levels and load resistance

Laboratory simulation experiments were performed on a system having two serially connected PV modules (sources) with the proposed MPPT algorithm and multilevel DC-Link converter as shown in Figure 1. Each module was exposed to a separate artificial sunlight with adjustable irradiance emulated by three halogen bulbs each of which was supplied from a different phase of a 3-phase variac connected to the 3-phase 50-Hz mains supply. This arrangement provides a fairly uniform irradiance to each module.

The parameters of the experimental system are listed in Table 5. The measured P-V characteristic of the PV module is shown in Figure 6 under different irradiance levels at room and surface temperatures of 20°C. The different irradiation levels can result in the different output characteristics of the components, and the variable load resistance (R_{load}) meanwhile affects the output characteristics. To evaluate the superiority of the proposed optimal control method, the proposed method is compared with the basic P&O method and the traditional PSO method under different shading patterns. The basic parameters used in the traditional PSO method and the proposed method are shown in Table 6.

It was tested under different illumination and load resistance values. The PSCs and load variation are divided into six cases, including: Case 1, setting G_1=250W/m² and G_2=500 W/m², where the R_{load} =20Ω; Case 2, setting G_1=250W/m² and G_2=800 W/m², where the R_{load} =17Ω; Case 3, setting G_1=500W/m² and G_2=800 W/m², where the R_{load} =8Ω; Case 4, setting G_1=1000W/m² and G_2=250 W/m², where the R_{load} =15Ω; Case 5, setting G_1=1000W/m² and G_2=500 W/m², where the R_{load}=6.5Ω; Case 6, setting G_1=1000W/m² and G_2=800 W/m², where the R_{load} =5Ω. What's more, the values used for the different PSCs and the variable R_{load} in each case are presented in Table 7, and f_r= 50 Hz, m_f=30 and C_{PV}= 5.5 mF, L_{load} = 5 mH. The frequency modulation index could be chosen to be even higher, if the equipment used allows it, in order to get even better results when it comes to harmonics. For comparison purposes, the total harmonics distortion (THD) along with the amplitude of 50Hz fundamental harmonicis is calculated for the first thousand harmonics.
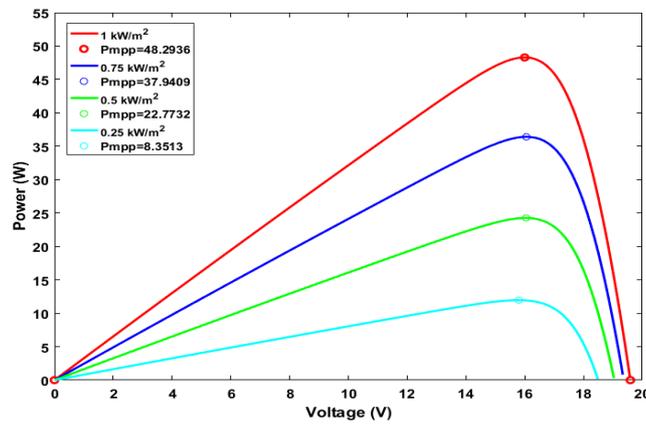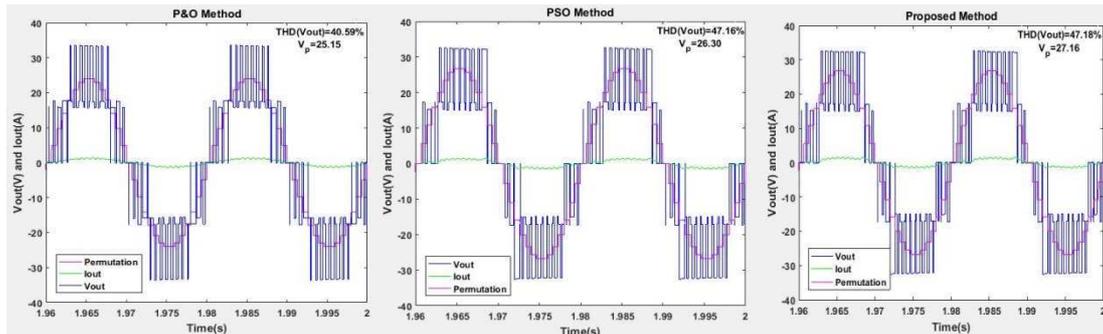

Figure 6 Measured P-V characteristics of the PV source for different irradiance levels (MPP
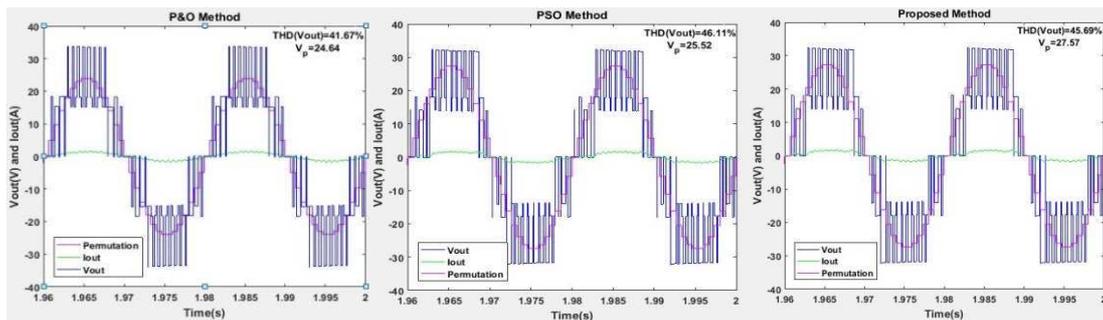
is indicated on each characteristic)

Table 7 R_{Load} variation value of each case of irradiance (at 20□)

Case	G_1 (W/m²)	G_2 (W/m²)	R_{load} (Ω)
1	250	500	20

2	250	800	17
3	500	800	8
4	1000	250	15
5	1000	500	6.5
6	1000	800	5

(a)

(b)

(c)

(d)

(e)

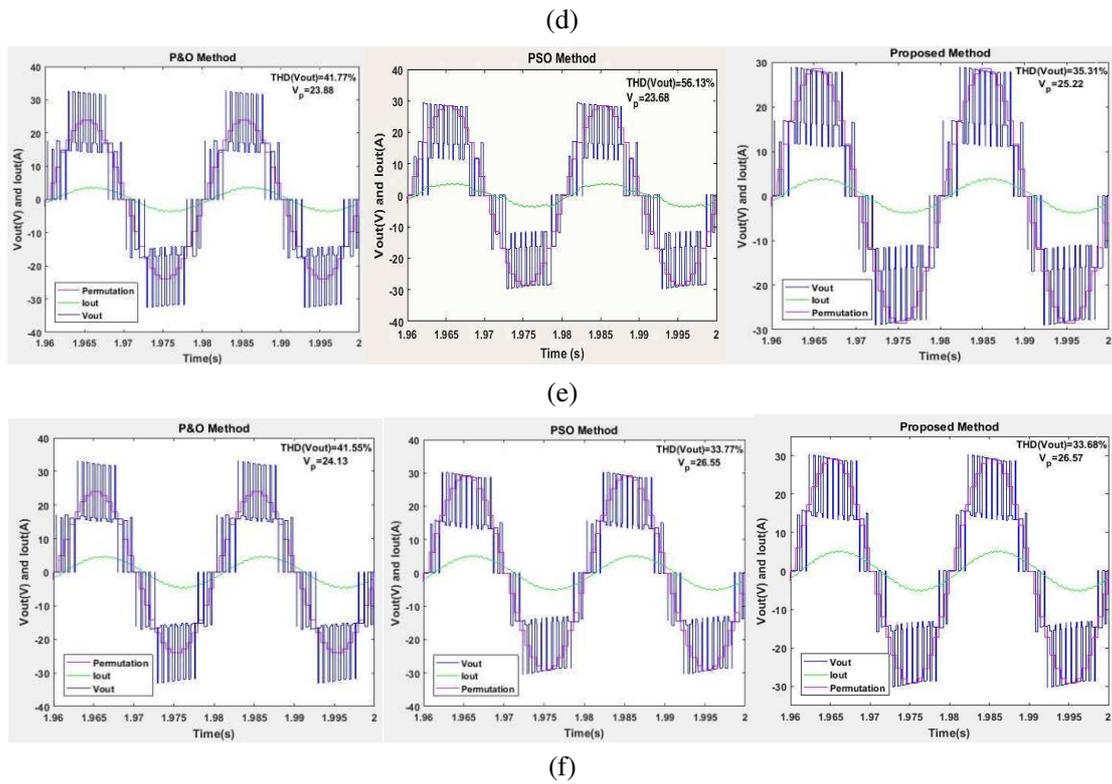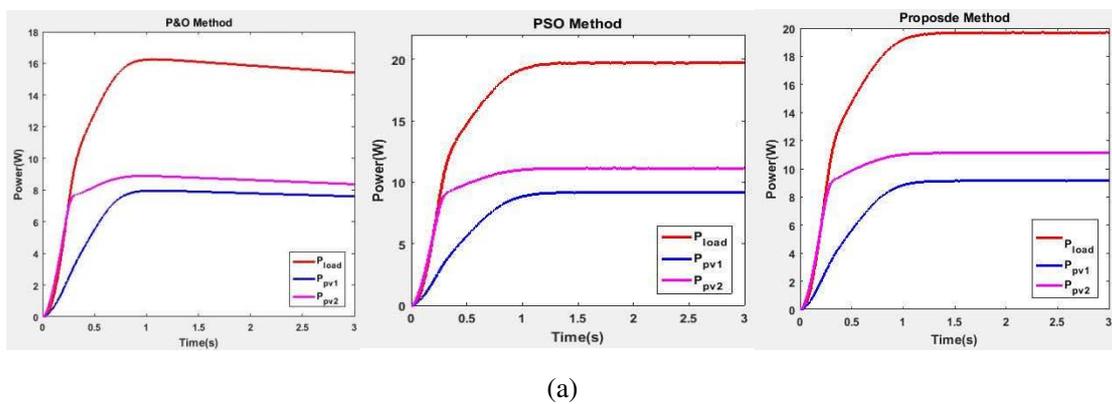

(f)
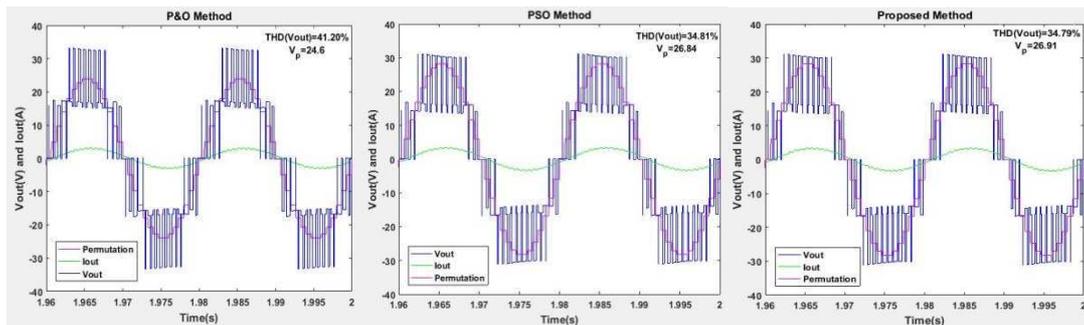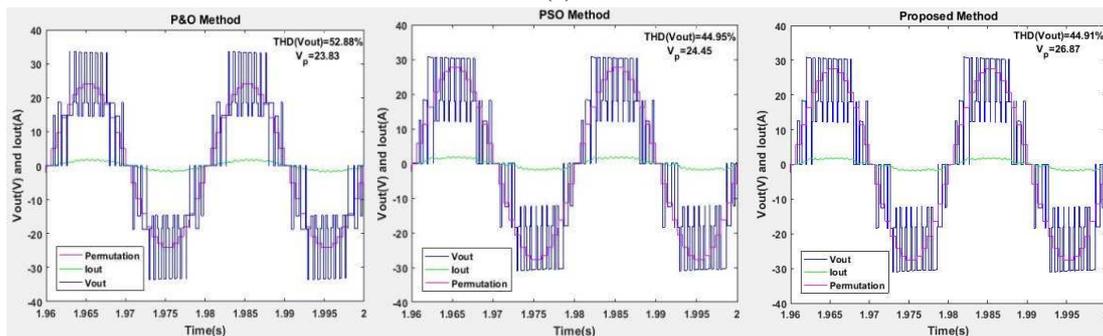
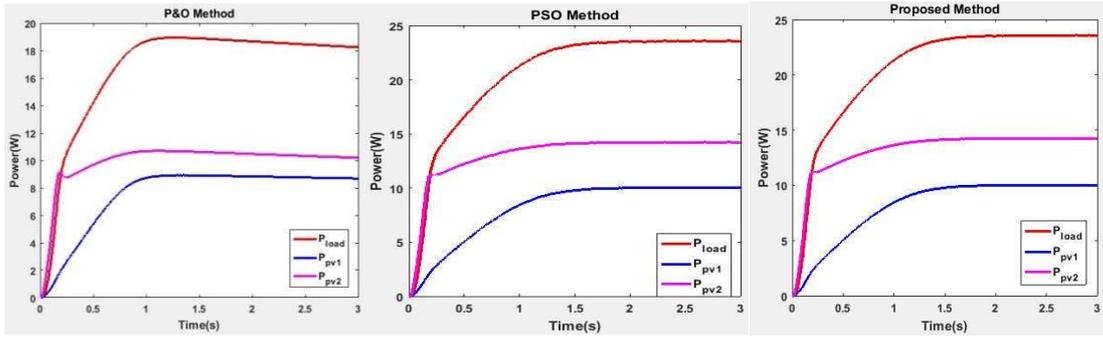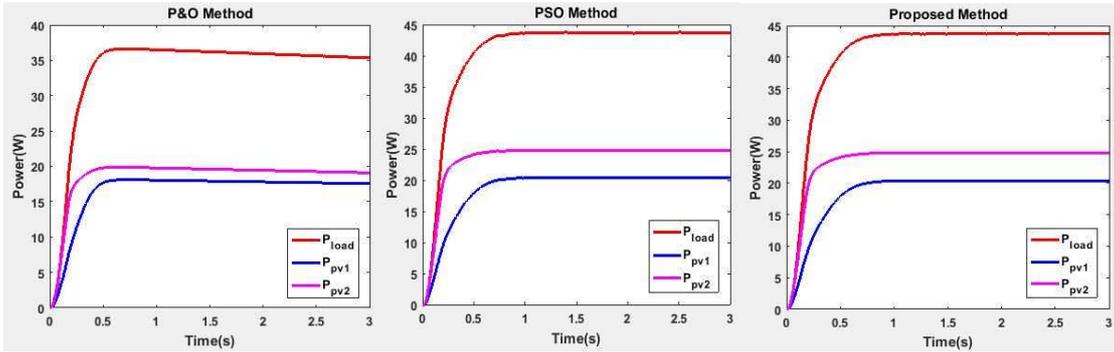Figure 7 Output voltage, current waveforms and permutations of five-level converter measured

under the control by P&O method (column 1), PSO method (column 2) and the

proposed method (columns 3). Irradiances in W/m^2 and load resistance values in Ω

applied to sources PV1 and PV2: (a) 250, 500, 20; (b) 250, 800, 17; (c) 500, 800, 8;

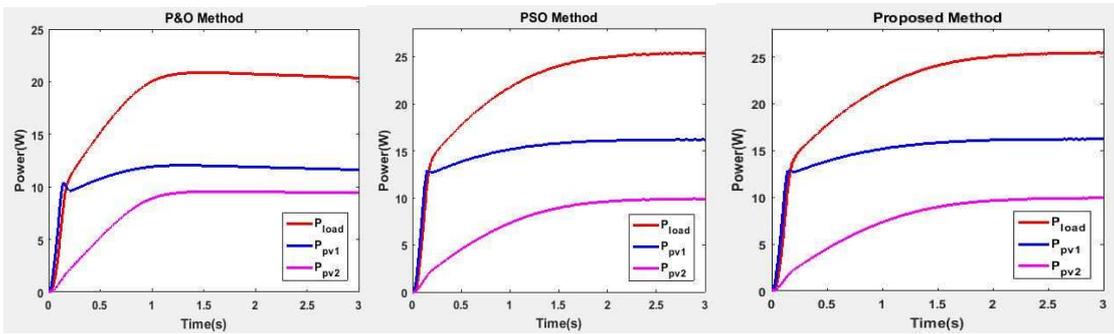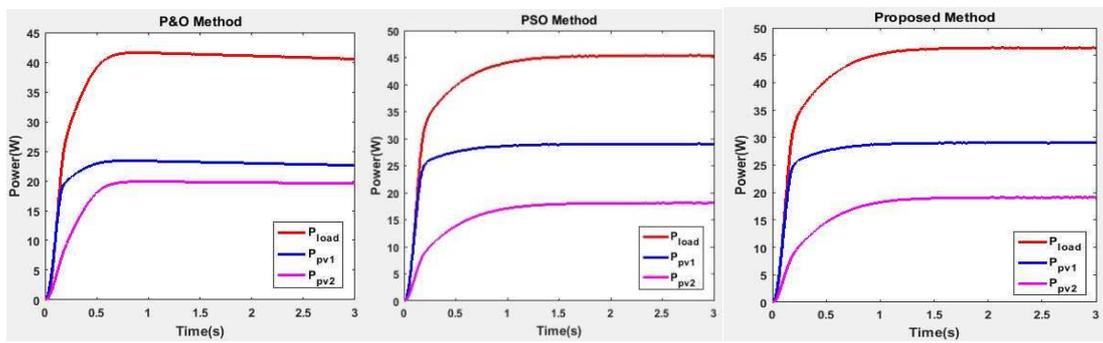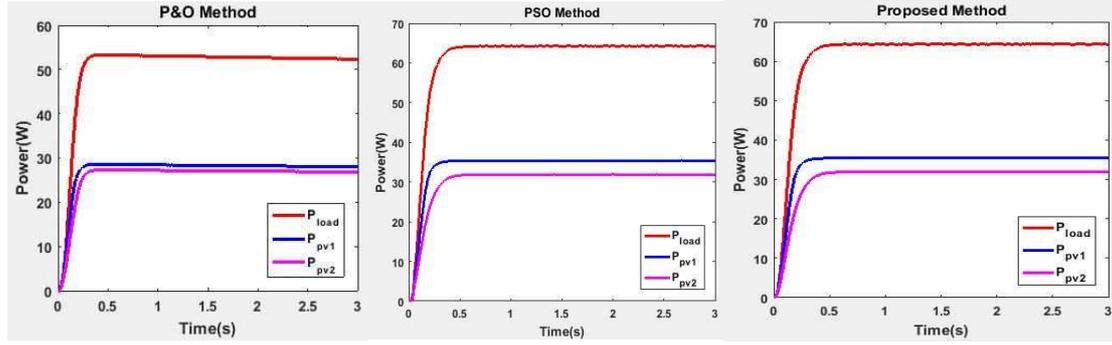(d) 1000, 250, 15; (e) 1000, 500, 6.5; (f) 1000, 800, 5.

(a)

(b)

(c)

(d)

(e)

(f)

Figure 8 Load power (P_{load}), pv1 power (P_{pv1}) and pv2 power (P_{pv2}) of five-level converter measured under the control by P&O method (column 1), PSO method (column 2) and the proposed method (columns 3). Irradiances in W/m² and load resistance values in Ω applied to sources PV1 and PV2: (a) 250, 500, 20; (b) 250, 800, 17; (c) 500, 800, 8; (d) 1000, 250, 15; (e) 1000, 500, 6.5; (f) 1000, 800, 5.

Table 8   Summary of simulated results at various shading levels

CASE	P&O method		PSO method		Proposed method	
	THD (%)	V_P(V)	THD (%)	V_P(V)	THD (%)	V_P(V)
1	40.59%	25.15	47.16%	26.30	47.18%	27.16
2	41.67%	24.64	46.11%	25.52	45.69%	27.57
3	41.20%	24.6	34.81%	26.84	34.79%	26.91
4	52.88%	23.83	45.98%	24.45	44.91%	26.87
5	41.77%	23.88	56.13%	23.68	35.31%	25.22
6	41.55%	24.13	33.77%	26.55	33.68%	26.57

Table 9 Measured values of power delivered to the load at different shading patterns

Case	P&O method (W)			PSO method (W)			Proposed method (W)		
	P_{pv1}	P_{pv2}	P_{Load}	P_{pv1}	P_{pv2}	P_{Load}	P_{pv1}	P_{pv2}	P_{Load}
1	7.96	8.89	16.26	9.20	11.16	19.76	9.22	11.19	19.80
2	8.92	10.69	18.94	10.04	14.25	23.61	10.02	14.24	23.59
3	18.10	19.89	36.63	20.45	24.82	43.80	20.42	24.83	43.77
4	12.04	9.56	20.87	16.22	9.92	25.41	16.24	9.94	25.47

5	23.41	19.90	41.60	29.07	18.13	45.47	29.08	19.11	46.40
6	28.55	27.28	53.28	35.44	31.94	64.39	35.47	31.94	64.44

Table 8 gives a comparison between the three algorithms in terms of the output quality, where the THD along with the amplitude of 50Hz fundamental harmonic are presented. From Table 8, it can be seen that although the THD of the proposed method is lower than the other two methods in Case 1 and Case 2, its output voltage is better. And, the output quality of the proposed method completely outperforms the other methods in the other Cases, which shows a lower output harmonic distortion of the proposed method. Furthermore, Figure 7 are plotted to show the 50Hz fundamental amplitude of the load voltage waveforms, load current waveforms and permutation waveforms, using the P&O, PSO and proposed methods as a function of the PV extracted power. Some significant conclusion can be obtained from Table 8 and Figure 7 that at the same conditions of partial shading and load resistance value, the proposed method has resulted in a lower output harmonic distortion and larger amplitude of the fundamental harmonic (50 Hz) compared to the other two methods in most cases.

What's more, Table 9 lists the output load power (P_{load}), respective output power (P_{pv1}) and (P_{pv2}) of the two PV arrays, and the output power curves are shown in Figure 8. From Table 9, we can find that although the output power of the PSO method is slightly higher in Case 3, but the proposed method is completely beyond the other method in other cases. By comparing and analyzing the curves in Figure 8, we can more clearly see that the proposed method outperforms the P&O and PSO methods in the same shading conditions, which indicates that the control scheme with the proposed method has a lower energy loss.

5 Conclusions

This paper described optimal control scheme for the single-phase grid-connected PV system under different fast variation shading patterns, which includes the proposed MPSO based-MPPT algorithm, DC/DC boost converter and a half-bridge ANPC inverter, is presented. The main features of the scheme are: i) combining the extended memory searching capabilities and the adaptive inertia weight of MPSO, MPSO is successfully performed by a boost DC/DC converter to quickly and accurately search for the MPP and hence reduce the voltage ripple and increase the power output under different partial shading conditions; ii) the PV system with multilevel DC link converters and a PWM permutation algorithm is used to validate the effectiveness of the control scheme. The proposed MPSO algorithm has been validated by means of stability analysis and numerical simulation analysis. Simulation results tested on the static and dynamic irradiance levels show the effectiveness of the proposed control scheme is effective in terms of the accuracy of the MPP tracking and the quality of the output waveforms, and can generate higher output power.

This paper only analyzes and applies the simulation of the proposed control scheme, so we will continue optimizing the proposed algorithm and the simulation experiment platform, using the multilevel DC link converters with seven-level AC output voltages and further completing the verification of the hardware platform in the future.

Acknowledgements

References

Alajmi, B. N., Ahmed, K. H., Finney, S. J., Williams, B. W., 2011. Fuzzy-logic-control approach of a modified hill-climbing method for maximum power point in microgrid standalone photovoltaic system. IEEE Trans. Power Electron. 26(4), 1022-1030.

Abdalla, I., Corda, J., Zhang, L., 2016. Optimal control of a multilevel DC-link converter photovoltaic system for maximum power generation. Renew. Energy 92, 1-11.

Boumaaraf, H., Talha, A., Bouhali, O., 2015. A three-phase NPC grid-connected inverter for photovoltaic applications using neural network MPPT. Renew. Sustain. Energy Rev. 49, 1171-1179.

Babu, T.S., Rajasekar, N., Sangeetha, K., 2015. Modified particle swarm optimization technique based maximum power point tracking for uniform and under partial shading condition. Appl. S. Comput. 34, 613-624.

Busquets-Monge, S., Rocabert, J., Rodríguez, P., Alepuz, S., Bordonau, J., 2008. Multilevel diode-clamped converter for photovoltaic generators with independent voltage control of each solar array. IEEE Trans. Ind. Electron. 55(7), 2713-2723.

Cheng, P.C., Peng, B.R., Liu, Y.H., Cheng, Y. S., Huang, J.W., 2015. Optimization of a fuzzy-logic-control-based MPPT algorithm using the particle swarm optimization technique. Energies 8(6), 5338-5360.

Duan, Q., Mao, M., Duan, P., Hu, B., 2016. An improved artificial fish swarm algorithm optimized by particle swarm optimization algorithm with extended memory. Kybernetes 45(2), 210-222.

Dai, N.Y., Wong, M.C., Chen, Y.H., Han, Y.D., 2005. A 3-D generalized direct PWM algorithm for multilevel converters. IEEE Power Electron. Let. 3(3), 85-88.

Elgendy, M.A., Zahawi, B., Atkinson, D.J., 2012. Assessment of Perturb and Observe MPPT algorithm implementation techniques for PV pumping applications. IEEE Trans. Sustain. Energy 3 (1), 21–33.

Elbaset, A.A., Ali, H., Abd-El, S.M., et al., 2016. Implementation of a modified perturb and observe maximum power point tracking algorithm for photovoltaic system using an embedded microcontroller. IET Renew. Power Gener. 10(4), 551-560.

Eberhart, R., Kennedy, J., 1995. A new optimizer using particle swarm theory. In Micro Machine and Human Science, Proceedings of the Sixth International Symposium on, 39-

43.

Eberhart, R.C., Shi, Y., 2004. Guest editorial special issue on particle swarm optimization. IEEE Trans. Evolut. Comput. 8(3), 201-203.

Gupta, A., Chauhan, Y.K., Pachauri, R.K., 2016. A comparative investigation of maximum power point tracking methods for solar PV system. Sol. Energy 136, 236-253.

Gao, L., Dougal, R.A., Liu, S., Iotova, A.P., 2009. Parallel-connected solar PV system to address partial and rapidly fluctuating shadow conditions. IEEE Trans. Ind. Electron. 56(5), 1548-1556.

Ishaque, K., Salam, Z., Amjad, M., Mekhilef, S., 2012. An improved particle swarm optimization (PSO)–based MPPT for PV with reduced steady-state oscillation. IEEE Trans. Power Electron. 27(8), 3627-3638.

Ishaque, K., Salam, Z., Shamsudin, A., Amjad, M., 2012. A direct control based maximum power point tracking method for photovoltaic system under partial shading conditions using particle swarm optimization algorithm. Appl. Energy 99, 414-422.

Killi, M., Samanta, S., 2015. Modified perturb and observe MPPT algorithm for drift avoidance in photovoltaic systems. IEEE Trans. Ind. Electron. 62 (9), 5549-5559.

Koad, R., Zobaa, A F., El Shahat, A., 2016. A Novel MPPT Algorithm Based on Particle Swarm Optimisation for Photovoltaic Systems. IEEE Trans. Sustain. Energy.

Kim, I.S., 2007. Robust maximum power point tracker using sliding mode controller for the three-phase grid-connected photovoltaic system. Sol. Energy 81(3), 405-414.

Li, C., Chen, Y., Zhou, D., et al., 2016. A High-Performance Adaptive Incremental Conductance MPPT Algorithm for Photovoltaic Systems. Energies 9(4), 288.

Letting, L. K., Munda, J. L., Hamam, Y., 2012. Optimization of a fuzzy logic controller for PV grid inverter control using S-function based PSO. Sol. Energy 86(6), 1689-1700.

Lin, F.J., Lu, K.C., Ke, T.H., 2016. Probabilistic Wavelet Fuzzy Neural Network based reactive power control for grid-connected three-phase PV system during grid faults. Renew. Energy 92, 437-449.

Liu, Y.H., Huang, S.C., Huang, J.W., Liang, W.C., 2012. A particle swarm optimization-based maximum power point tracking algorithm for PV systems operating under partially shaded conditions. IEEE Trans. Energy Convers. 27(4), 1027-1035.

Liu, L., Meng, X., Liu, C., 2016. A review of maximum power point tracking methods of PV power system at uniform and partial shading. Renew. Sustain. Energy Rev. 53, 1500-1507.

Messai, A., Mellit, A., Guessoum, A., Kalogirou, S. A., 2011. Maximum power point tracking using a GA optimized fuzzy logic controller and its FPGA implementation. Sol. energy 85(2), 265-277.

Manickam, C., Raman, G.R., Raman, G.P., Ganesan, S.I., Nagamani, C., 2016. A Hybrid Algorithm for Tracking of GMPP Based on P&O and PSO With Reduced Power Oscillation in String Inverters. IEEE Trans. Ind. Electron. 63(10), 6097-6106.

Mojallizadeh, M.R., Badamchizadeh, M., Khanmohammadi, S., Sabahi, M., 2016. Designing a new robust sliding mode controller for maximum power point tracking of photovoltaic cells. Sol. Energy 132, 538-546.

Middlebrook, R.D., Cuk, S., 1976. A general unified approach to modelling switching-converter power stages. In Power Electronics Specialists Conference, 18-34.

Radjai, T., Rahmani, L., Mekhilef, S., Gaubert, J. P., 2014. Implementation of a modified incremental conductance MPPT algorithm with direct control based on a fuzzy duty cycle change estimator using dSPACE. Sol. Energy 110, 325-337.

Rezvani, A., Gandomkar, M., 2016. Modeling and control of grid connected intelligent hybrid photovoltaic system using new hybrid fuzzy-neural method. Sol. Energy 127, 1-18.

Rezk, H., Eltamaly, A.M., 2015. A comprehensive comparison of different MPPT techniques for photovoltaic systems. Sol. energy 112, 1-11.

Renaudineau, H., Donatantonio, F., Fontchastagner, J., Petrone, G., Spagnuolo, G., Martin, J. P., Pierfederici, S., 2015. A PSO-based global MPPT technique for distributed PV power generation. IEEE Trans. Ind. Electron. 62(2), 1047-1058.

Shimizu, T., Hirakata, M., Kamezawa, T., Watanabe, H., 2001. Generation control circuit for photovoltaic modules. IEEE Trans. Power Electron. 16(3), 293-300.

Sundareswaran, K., Palani, S., 2015. Application of a combined particle swarm optimization and perturb and observe method for MPPT in PV systems under partial shading conditions. Renew. Energy 75, 308-317.

Seyedmahmoudian, M., Rahmani, R., Mekhilef, S., Oo, A.M.T., Stojcevski, A., Soon, T.K., Ghandhari, A.S., 2015. Simulation and hardware implementation of new maximum power point tracking technique for partially shaded PV system using hybrid DEPSO method. IEEE Trans. Sustain. Energy 6(3), 850-862.

Shi, Y., Eberhart, R., 1998. A modified particle swarm optimizer. In Evolutionary Computation Proceedings, IEEE World Congress on Computational Intelligence., The 1998 IEEE International Conference on , 69-73.

Shi, Y., Eberhart, R.C., 1998. Parameter selection in particle swarm optimization. In International Conference on Evolutionary Programming, 591-600.

Shi, Y., Eberhart, R.C., 1999. Empirical study of particle swarm optimization. In Evolutionary Computation, Proceedings of the 1999 Congress on, 3,1945-1950.

Velasco-Quesada, G., Guinjoan-Gispert, F., Piqué-López, R., Román-Lumbreras, M., Conesa-Roca, A., 2009. Electrical PV array reconfiguration strategy for energy extraction improvement in grid-connected PV systems. IEEE Trans. Ind. Electron. 56(11), 4319-4331.

Wu, H., Nie, C., Kuo, F.C., Leung, H., Colbourn, C.J., 2015. A discrete particle swarm optimization for covering array generation. IEEE Trans. Evolut. Comput. 19(4), 575-591.

Xiao, X., Huang, X., Kang, Q., 2016. A Hill-Climbing-Method-Based Maximum-Power-Point-Tracking Strategy for Direct-Drive Wave Energy Converters. IEEE Trans. Ind. Electron. 63(1), 257-267.

Zhan, Z.H., Zhang, J., Li, Y., Chung, H.S.H., 2009. Adaptive particle swarm optimization. IEEE Trans. Sys. Man Cyber. Part B (Cybernetics) 39(6), 1362-1381.

Zou, R., Kalivarapu, V., Winer, E., Oliver, J., Bhattacharya, S., 2015. Particle swarm optimization-based source seeking. IEEE Trans. Auto. Sci. Eng. 12(3), 865-875.